NUCL SCI TECH (2018) 29:8
https://doi.org/10.1007/s41365-017-0353-1

Effect of current intensity on radiological properties of joined 304L stainless steels for photon interaction

Mehmet Büyükyıldız[1]

Received: 20 February 2017 / Revised: 21 April 2017 / Accepted: 26 April 2017 / Published online: 22 December 2017

Abstract Radiological properties, such as the linear attenuation coefficient (μ), mass attenuation coefficient (μ/ρ), half-value layer (HVL), tenth-value layer (TVL), mean free path (MFP), and effective atomic number (Z_{eff}), of 304L stainless steels have been investigated with respect to photon interactions to determine the influence of current intensity at different gamma-ray energies. ^{137}Cs and ^{60}Co radioactive point sources were used to irradiate 304L stainless steels joined at 45–70-A weld currents for the transmission of the gamma rays at photon energies of 661.0, 1173.2, and 1332.5 keV. The μ, μ/ρ, HVL, TVL, MFP, and Z_{eff} of the steels were measured at the mentioned energies, and theoretical values for pure 304L stainless steel were calculated for comparison. The minimum differences (%) in Z_{eff} between pure steel and steel joined at a weld current of 60 A were observed for relevant photon energies; the minimum difference between the theoretical value for pure 304L and the experimental value for joined steel was 4.76%, and that between the experimental value for pure 304L and the experimental value for joined steel was 2.60% at 1332.5 keV. Moreover, the MFPs of the joined steels were compared with that of pure 304L, and steel joined at 60 A, which had the minimum MFP, was compared with some radiation-shielding concretes in terms of MFP at the same gamma-ray energies.

This work was supported by the Yalova University Scientific Research Foundation (No. 2013-062).

✉ Mehmet Büyükyıldız
m.buyukyildiz@gmail.com

[1] Department of Electrical and Electronics, Faculty of Engineering, Yalova University, Yalova, Turkey

Keywords Effective atomic number · Mean free path · 304L stainless steel

1 Introduction

Stainless steels are widely used in different fields such as the automotive industry, engineering, structural materials, and nuclear technology because of their excellent microstructural, mechanical, and physical properties. In addition, stainless steels such as 304L have a promising shielding property due to the presence of heavy metals such as Cr, Fe, Ni, and Cu. Thus, these materials are extensively used for shielding in nuclear reactors, nuclear power plants, medical and radiation research centers, etc. Welding is a fabrication process used to join materials and is an important research issue in relation to 304L or other such steels because of various applications such as nuclear technology. Materials can be joined to determine the parameters of the welding process and to compare base materials or others in terms of microstructural, mechanical, and physical properties [1, 2]. The current intensity is one of the most important parameters affecting mechanical or physical properties in the welding process [3].

The microstructural, mechanical, and physical properties of 304L stainless steel have been widely studied with respect to the tensile strength, engineering stress, cooling effects, microhardness, current or voltage effects, etc., of the welding process [4–18]. Furthermore, the influence of weld current on the welding process was investigated by some researchers. Ozyurek observed the effects of weld current (in the range of 4–9 kA) and weld atmosphere on some properties of 304L steel [19], and he reported that the optimum welding parameters producing the maximum joint strength were established at a weld current of 9 kA. The influence of current intensity and heat input on thin zinc-coated TRIP 800 steel plates was studied at different welding conditions such as current intensities in the range of 45–80 A [3]. Apart from the mechanical or microstructural properties of stainless steels, some physical parameters such as the linear attenuation coefficient (μ), mass attenuation coefficient (μ/ρ), half-value layer (HVL), tenth-value layer (TVL), mean free path (MFP), and effective atomic number (Z_{eff}) are very important to design or produce new materials for shielding in nuclear physics research, nuclear engineering, and nuclear reactors. Several theoretical and experimental studies have been conducted on the gamma-ray shielding of stainless steels. Akkurt determined the photon interaction parameters of three different steels at photon energies of 662, 1173, and 1332 keV [20]. The results were compared to theoretical results, and the relation between these parameters and the gamma-ray energy was discussed in detail. Singh and Badiger theoretically investigated the radiation interaction properties (mass attenuation coefficients, effective atomic numbers, and electron densities) of carbon and stainless steels in the energy region of 1 keV–100 GeV [21]. The obtained values were compared to experimental results in the literature, and they reported that the effective atomic numbers of 304L obtained by different methods in the study were equal. The radiological properties such as mass attenuation coefficients, effective atomic numbers, and electron densities of some carbon and stainless-steel alloys were calculated using Geant4 and Monte Carlo n-particle (MCNP) simulation codes at different source energies, and the results were compared with theoretical (using the WinXCom program) and experimental results [22]. Radiation-shielding parameters such as effective atomic numbers and electron densities of oxide-dispersion-strengthened steels were theoretically investigated, and variations in these parameters were evaluated in a continuous energy region [23]. The attenuation capability of manganese austenitic stainless steel for fusion reactor systems was investigated in terms of photon and neutron interactions by using ^{60}Co and ^{232}Th radioactive sources, and the results obtained with the two sources were compared with each other [24]. However, to our knowledge, there is no study in the literature on welding zones or areas in terms of the radiation attenuation of materials, especially with respect to parameters of the welding process such as current intensity. Because the welding areas of joined materials are exposed to radiation, such as the base material in any radiation application, it is important to investigate the radiation response of welding areas. This was the motivation for the present study.

2 Method

The mass attenuation coefficient of a compound or mixture can be obtained by the Beer–Lambert law at any photon energy by,

$$\mu_{\mathrm{m}} = \left(\frac{\mu}{\rho}\right) = \frac{\ln(I_0/I)}{\rho t} \tag{1}$$

$$I = I_0 e^{-\mu x} = I_0 e^{-\mu_{\mathrm{m}} t}, \tag{2}$$

where I_0 and I are unattenuated and attenuated photons intensities, respectively; μ (cm^{-1}) and μ_{m} (cm^2 g^{-1}) are linear and mass attenuation coefficients, respectively; x (cm) and t (g cm^{-2}) are the thickness and sample mass thickness (the mass per unit area), respectively; and ρ (gcm^{-3}) is the density of the material. The total mass attenuation coefficient μ_{m} for any composite of elements is given by the mixture rule:

$$\mu_{\mathrm{m}} = \left(\frac{\mu}{\rho}\right) = \sum_i w_i (\mu/\rho)_i, \tag{3}$$

where $w_i = n_i A_i / \sum_i n_i A_i$ is the mass fraction of the ith constituent element, A_i is the atomic weight of the ith element, and n_i is the number of atoms of ith constituent element in the composite [25]. For determining theoretical mass attenuation coefficients or total atomic cross sections, the WinXCom computer program was used [26]. HVL and TVL refer to the thickness of the material at which the intensity of incident radiation is reduced by one half and one-tenth, respectively, and MFP is the average distance between two successive interactions. These parameters can be calculated using the linear attenuation coefficient (μ) according to the following equations:

$$\mathrm{HVL} = \frac{\ln(2)}{\mu} = \frac{0.693}{\mu},\ \mathrm{TVL} = \frac{\ln(10)}{\mu} = \frac{2.302}{\mu},\ \text{and MFP} = \frac{1}{\mu}. \tag{4}$$

The total photon interaction cross section (σ_t) for materials can be obtained from the measured mass attenuation coefficients μ_{m} using the following equation:

$$\sigma_t = \frac{\mu_{\mathrm{m}} \sum_i n_i A_i}{N_A}, \tag{5}$$

where N_A is the Avogadro number. Furthermore, the total atomic (σ_{a}) and electronic (σ_{e}) cross sections can be calculated as follows:

$$\sigma_{\mathrm{a}} = \frac{\sigma_t}{\sum_i n_i} \text{ and } \sigma_{\mathrm{e}} = \frac{1}{N_A} \sum \frac{f_i A_i}{Z_i} (\mu_{\mathrm{m}})_i, \tag{6}$$

where f_i is the fractional abundance of the ith element with respect to the number of atoms, and Z_i is the atomic number of the ith element. Finally, the effective atomic number of the material can be determined using the total atomic and electronic cross sections through the following relation:

$$Z_{\mathrm{eff}} = \frac{\sigma_a}{\sigma_e}. \tag{7}$$

3 Experimental

In the present study, welding conditions for steels comprised wire feed speeds of 2.2–3.7 m/min, arc voltages of 11.7–12.4 V, a shielding gas flow rate of 12 L/min, a brazing travel speed of 24 cm/min, and a brazing gap of 0.5 mm. Under these conditions, which were constant for all measurements, the steel plates of 1 mm thickness were joined using six different weld currents: 45, 50, 55, 60, 65, and 70 A. A sample steel plate joined with the metal inert gas (MIG) brazing technique at 60 A and its microstructure are shown in Fig. 1 (10 × 10 mm) as an example. The chemical compositions of 304L steel (7.84 g/cm^3) and the welding wire ($CuAl_8$) are listed in Table 1, and those of the joined steels are listed in Table 2.

The experimental arrangement is shown in Fig. 2. In order to obtain attenuated and unattenuated intensities, all specimens were irradiated using 661.66-, 1173.23-, and 1332.50-keV gamma rays emitted from ^{137}Cs and ^{60}Co point radioactive sources, which have activities of 8.83 and 3.52 µC, respectively. Attenuated and unattenuated peaks emitted from the targets were detected by a 3″ × 3″ NaI(Tl) detector (model 905-4 Ortec-Ametek). The photomultiplier tube (PMT) base, digiBASE (Ortec), has a diameter and length of 6.3 and 8.0 cm, respectively. The FWHM was equal to 46 keV at 662 keV and 65 keV at 1330 keV. PMT is separated from the NaI crystal by a 5-mm-thick glass window. The photodetector is protected by a 0.05-mm-thick aluminum housing separated from the crystal by a very thin air gap. The thickness of air between the aluminum and crystal and between the aluminum and photomultiplier is 0.25 mm at the sides and 0.2 mm at the top and bottom. The dimensions of the integral unit in its

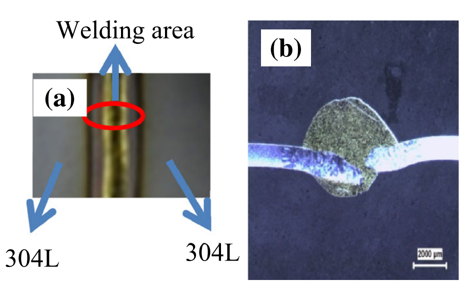

Fig. 1 (Color online) Images of joined area and its microstructure (at a weld current of 60 A) of 304L stainless steel

Table 1 Chemical compositions of 304L steel and copper-based wire ($CuAl_8$)

C	Si	Mn	P	S	Cr	Ni	N	Fe
304L stainless steel								
0.021	0.38	1.80	0.33	0.002	18.20	9.10	0.054	rest

Al	Mn	Fe	Sn	Cu
Welding wire				
8.0	< 0.5	< 0.5	< 0.5	Rest

casing are 22.35 cm in length, 8.2 cm in diameter at the crystal part, and 5.8 cm in diameter at the photomultiplier part. All data were analyzed using the Genie-2000 software. The data were collected into a multichannel analyzer (MCA) with 4096 channels and further analyzed using the demo version of Origin 7.5 software program.

4 Results and discussion

The error was determined from errors in the number of counts read by the software and in measuring the thickness of materials, as given as follows [27]:

$$\Delta\mu = \frac{1}{x}\sqrt{\left(\frac{\Delta I_0}{I_0}\right)^2 + \left(\frac{\Delta I}{I}\right)^2 + \ln\left(\frac{I_0}{I}\right)^2 \left(\frac{\Delta x}{x}\right)^2}. \tag{8}$$

From this equation, the error in linear attenuation coefficients was found to be within 3%. The welding process is very important, and its parameters such as current intensity and weld atmosphere can affect the similarities or dissimilarities between the base material and welding area in terms of mechanical and physical properties such as radiological properties. To show this effect, the samples obtained from the welding area of 304L stainless steels joined at weld currents of 45, 50, 55, 60, 65, and 70 A were irradiated using ^{137}Cs and ^{60}Co radioactive point sources. Then, attenuated and unattenuated intensities were measured at the source energies. The typical spectra of gamma rays with and without attenuation by the sample joined at 60 A are shown for the ^{137}Cs source in Fig. 3.

The linear attenuation coefficient (μ), mass attenuation coefficient (μ/ρ), HVL, TVL, and MFP of pure (theoretical) and joined 304L stainless steels for different photon energies are listed in the weld-current range of 45–70 A in Table 3. It can be seen from the table that the linear and mass attenuation coefficients depend on the photon energy and decrease with increasing photon energy. This is due to fact that more photons are attenuated at lower photon energies, while the probability of photon attenuation is reduced with the increase of photon energy [28]. HVL and

Table 2 Chemical compositions of joined 304L steels (welding area) from X-ray fluorescence

J. steels (A)	C	N	Al	Si	P	S	Cr	Mn	Fe	Ni	Cu	Sn
45	0.010	0.044	11.257	0.935	1.450	0.001	12.454	1.550	48.025	3.048	21.231	0.002
50	0.022	0.030	9.257	0.935	1.550	0.002	13.554	1.750	50.135	3.548	19.221	0.001
55	0.015	0.035	9.257	0.535	0.505	0.001	11.454	1.250	53.235	3.608	20.111	0.002
60	0.018	0.038	7.557	0.535	0.505	0.002	13.454	1.050	48.585	3.248	25.011	0.001
65	0.010	0.013	9.557	0.835	0.535	0.001	14.454	0.705	46.585	3.508	23.801	0.002
70	0.019	0.027	10.557	0.635	0.305	0.001	18.454	1.060	40.565	9.548	18.831	0.002

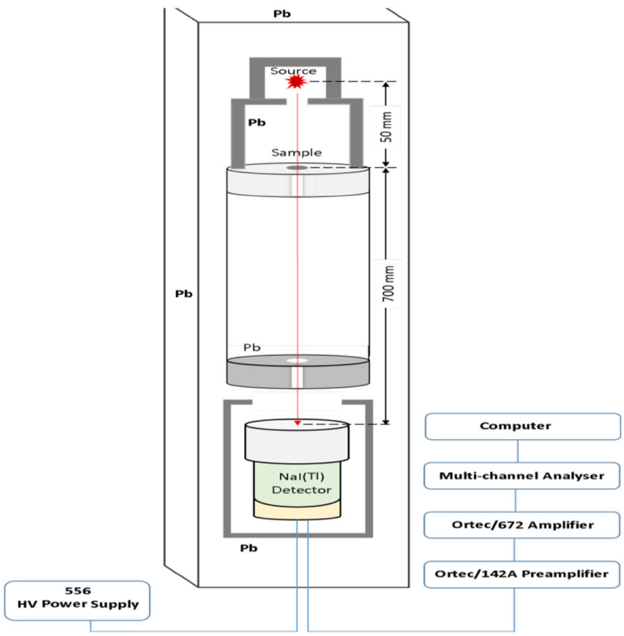

Fig. 2 (Color online) Experimental set up for the transmission of gamma rays

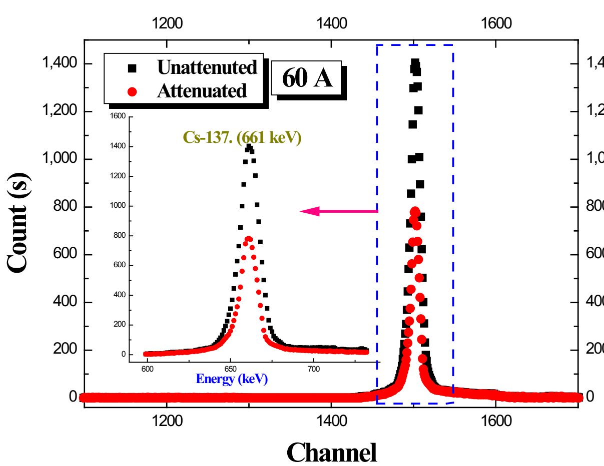

Fig. 3 (Color online) Typical spectrum of rays attenuated and unattenuated by steel (at a weld current of 60 A) for a ^{137}Cs source

Table 3 μ, (μ/ρ), HVL, TVL, and MFP of 304L and joined steels for different photon energies at various current intensities

keV	304L (Th)	45 A	50 A	55 A	60 A	65 A	70 A
μ							
661.0	0.554	0.493	0.502	0.502	0.527	0.525	0.523
1173.2	0.417	0.375	0.381	0.381	0.382	0.382	0.380
1332.5	0.391	0.354	0.358	0.359	0.366	0.360	0.358
μ/ρ(cm^2/g)							
661.0	0.074	0.067	0.067	0.067	0.069	0.069	0.069
1173.2	0.054	0.051	0.051	0.051	0.051	0.051	0.051
1332.5	0.052	0.048	0.048	0.048	0.048	0.048	0.048
HVL							
661.0	1.251	1.405	1.382	1.381	1.318	1.319	1.325
1173.2	1.663	1.851	1.820	1.818	1.815	1.817	1.822
1332.5	1.773	1.960	1.935	1.931	1.895	1.927	1.938
TVL							
661.0	4.155	4.667	4.590	4.589	4.378	4.383	4.400
1173.2	5.523	6.148	6.045	6.038	6.033	6.035	6.053
1332.5	5.891	6.511	6.426	6.414	6.294	6.402	6.438
MFP							
661.0	1.804	2.027	1.993	1.993	1.903	1.903	1.911
1173.2	2.399	2.670	2.625	2.622	2.621	2.621	2.629
1332.5	2.558	2.828	2.791	2.785	2.734	2.781	2.796

TVL are also very useful to identify a suitable specimen for gamma-ray shielding applications, and lower HVL and TVL values are required in applications for better radiation shielding. The values of HVL and TVL of pure (theoretical) and joined 304L stainless steels at different weld currents for the same photon energies are listed in Table 3. Generally, the values of HVL and TVL increase with increasing photon energy, as is expected based on the attenuation coefficients. In addition, the table indicates that HVL and TVL decrease with weld current from 45 to 60 A, and they have the minimum values at 60 A (difference (%) between pure (theoretical) and joined 304L stainless steels is minimum). This may be due to fact that different current intensities result in different heat inputs in the welding area

[3], causing different melting chemical compositions, as indicated in Table 2, because the other welding conditions are constant for all welding processes. Furthermore, it is well known that shielding parameters such as attenuation coefficients depend on the chemical composition and incident photon energy [20, 21, 27]. Table 3 also lists the MFP values of the investigated materials, which show the same energy and weld-current dependences as HVL and TVL because of the relation to the attenuation coefficients. The differences (%) in MFP between pure (theoretical) and joined 304L stainless steels at different weld currents were calculated at the same photon energies, as shown in Fig. 4. It can be clearly seen from this figure that the minimum differences (%) in MFP were observed at a weld current of 60 A for different photon energies. The obtained MFP results are compared with the MFP values of some standard radiation-shielding concretes at the same photon energies in Fig. 5 [29]. The figure shows that ilmenite has the lowest MFP among the shielding concretes, but base and joined (at 60 A) 304L steels have even lower MFP values. This is because the steels have higher densities than the corresponding shielding concretes, which have densities in the range of 2.30–3.50 g/cm^3. Therefore, it can be reported here that because of the lower MFP values, pure and joined 304L steels are better radiation-shielding materials than standard shielding concretes.

The effective atomic numbers of materials were determined at the studied photon energies and different weld currents, as listed in Table 4. The table indicates that the effective atomic numbers of joined 304L stainless steels increase with increasing gamma-ray energy from 661 to 1332 keV because the cross section of the photoelectric process varies inversely with the incident photon energy [30]. In addition, the maximum values of effective atomic number were observed at a weld current of 60 A, at which

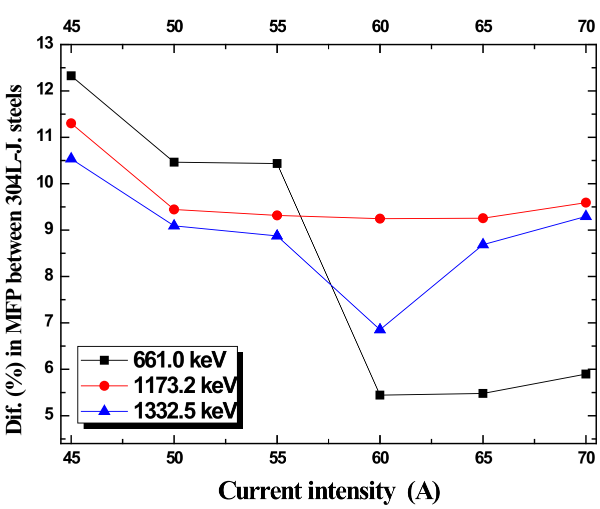

Fig. 4 (Color online) Differences (%) in MFP between pure (theoretical) and joined 304L stainless steels at different weld currents

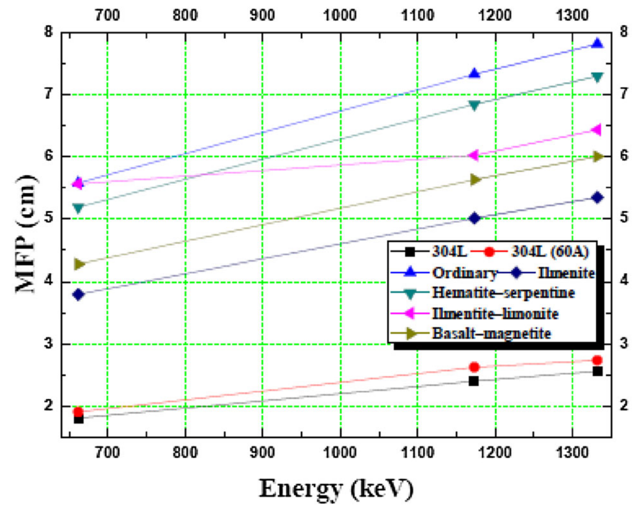

Fig. 5 (Color online) Values of MFP for pure and joined (at a weld current of 60 A) steels and those of some standard concretes

Table 4 Z_{eff} values of materials at different photon energies

Th	661.0 (keV)	1173.2 (keV)	1332.5 (keV)
304L	25.62	25.62	25.62
Exp			
304L	24.85	24.96	25.05
45 A	23.11	23.18	23.33
50 A	23.48	23.63	23.70
55 A	23.58	23.76	23.85
60 A	24.04	24.26	24.40
65 A	23.61	23.75	23.86
70 A	23.42	23.58	23.64

the value of Z_{eff} is the nearest to that of base 304L steel at all photon energies. The differences (%) in Z_{eff} between 304L (theoretical) and joined (experimental) steels, and between 304L (experimental) and joined (experimental) steels were calculated at different gamma-ray energies for comparison, as shown in Figs. 6 and 7. It can be clearly seen from the figures that the minimum differences (%) in Z_{eff} between 304L (theoretical or experimental) and joined (experimental) steels were observed at a weld current of 60 A for all photon energies, and the differences (%) in Z_{eff} between experimental results are smaller than between experimental and theoretical results.

5 Conclusion

In the present study, the linear attenuation coefficient (μ), mass attenuation coefficient (μ/ρ), HVL, TVL, MFP, and effective atomic number (Z_{eff}) of 304L stainless steels

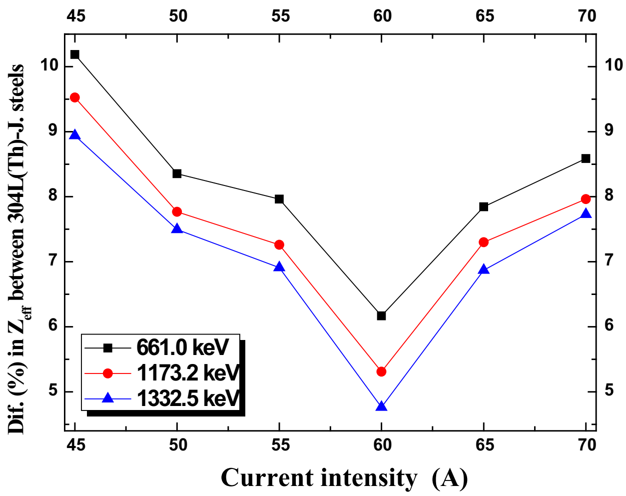

Fig. 6 (Color online) Differences (%) in Z_{eff} between 304L (theoretical) and joined (experimental) steels at different gamma-ray energies

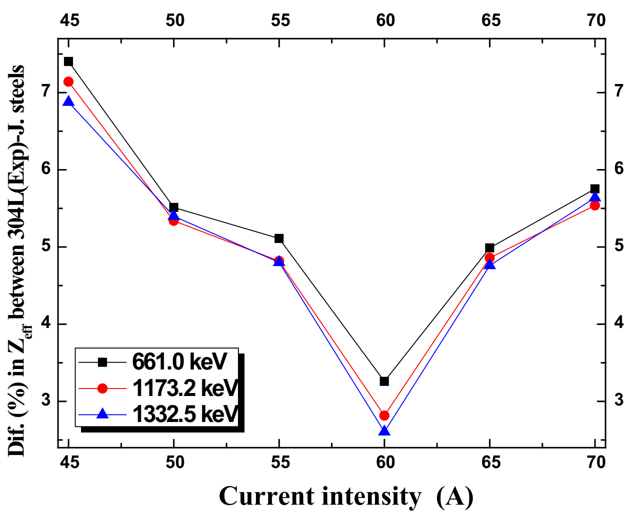

Fig. 7 (Color online) Differences (%) in Z_{eff} between 304L (experimental) and joined (experimental) steels at different gamma-ray energies

joined at weld currents in the range of 45–70 A have been investigated with respect to photon interactions to show the influence of current intensity for the first time. By investigating the materials in terms of radiation response, we found that differences in shielding parameters are an important factor for developing a new production process involving welding and for the design of materials because it is desired that base and joined materials show similar features with regard to mechanical and/or physical parameters. The minimum differences (%) in MFP between base 304L (theoretical) and joined 304L (experimental) steels were observed at a weld current of 60 A as 5.44, 9.24, and 6.85% at photon energies of 661, 1173, and 1332 keV, respectively. Furthermore, the minimum differences (%) in Z_{eff} between pure and joined 304L steels were observed at a weld current of 60 A for relevant photon energies; the minimum differences between 304L (theoretical) and joined (experimental) steels were 6.17, 5.31, and 4.76%, and between 304L (experimental) and joined (experimental) steels were 3.26, 2.81, and 2.60% at 661, 1173, and 1332 keV, respectively. From the results, it can be said that a weld current of 60 A is optimum for welding 304L stainless steel (with the MIG brazing technique) in terms of radiation-shielding properties, if the other welding conditions such as gas flow rate are almost constant, thus cannot be considered as a true constant. The effects of other welding parameters such as weld atmosphere on radiation interaction or shielding should be very interesting to study; more experimental data are required to clarify such effects.

References

1. A.E. Richard, *Pay attention to dissimilar-metal welds* (Avery Consulting Associates Inc., 2003). pp. 1–6
2. M. Shakil, M. Ahmad, N.H. Tariq et al., Microstructure and hardness studies of electron beam welded Inconel 625 and stainless steel 304L. Vacuum **110**, 121–126 (2014). https://doi.org/10.1016/j.vacuum.2014.08.016
3. F. Varol, E. Ferik, U. Ozsarac et al., Influence of current intensity and heat input in Metal Inert Gas-brazed joints of TRIP 800 thin zinc coated steel plates. Mater. Des. **52**, 1099–1105 (2013). https://doi.org/10.1016/j.matdes.2013.06.054
4. X.K. Zhu, Y.J. Chao, Numerical simulation of transient temperature and residual stresses in friction stir welding of 304L stainless steel. J. Mater. Process. Technol. **146**, 263–272 (2004). https://doi.org/10.1016/j.jmatprotec.2003.10.025
5. N. Ozdemir, Investigation of the mechanical properties of friction-welded joints between AISI 304L and AISI 4340 steel as a function rotational speed. Mater. Lett. **59**, 2504–2509 (2005). https://doi.org/10.1016/j.matlet.2005.03.034
6. G. Ruckert, B. Huneau, S. Marya, Optimizing the design of silica coating for productivity gains during the TIG welding of 304L stainless steel. Mater. Des. **28**, 2387–2393 (2007). https://doi.org/10.1016/j.matdes.2006.09.021
7. S.A.A. Akbari Mousavi, R. Miresmaeili, Experimental and numerical analyses of residual stress distributions in TIG welding process for 304L stainless steel. J. Mater. Process. Technol. **208**, 383–394 (2008). https://doi.org/10.1016/j.jmatprotec.2008.01.015
8. D.J. Lee, J.C. Byun, J.H. Sung et al., The dependence of crack properties on the Cr/Ni equivalent ratio in AISI 304L austenitic stainless steel weld metals. Mater. Sci. Eng. A **513–514**, 154–159 (2009). https://doi.org/10.1016/j.msea.2009.01.049
9. Z. Lu, T. Shoji, T. Dan et al., The effect of roll-processing orientation on stress corrosion cracking of warm-rolled 304L stainless steel in oxygenated and deoxygenated high temperature pure water. Corros. Sci. **52**, 2547–2555 (2010). https://doi.org/10.1016/j.corsci.2010.03.027
10. S. Taheri, A. Hauet, L. Taleb et al., Micro–macro investigations about the fatigue behavior of pre-hardened 304L steel. Int. J. Plast. **27**, 1981–2004 (2011). https://doi.org/10.1016/j.ijplas.2011.06.004

11. N. Haddar, A. Koster, Y. Kchaou et al., Thermal–mechanical and isothermal fatigue of 304L stainless steel under middle range temperatures. CR Mec. **340**, 444–452 (2012). https://doi.org/10.1016/j.crme.2012.02.015
12. S.K. Lawrence, D.P. Adams, D.F. Bahr et al., Mechanical and electromechanical behavior of oxide coatings grown on stainless steel 304L by nanosecond pulsed laser irradiation. Surf. Coat. Technol. **235**, 860–866 (2013). https://doi.org/10.1016/j.surfcoat.2013.09.013
13. G.R. Mirshekari, E. Tavakoli, M. Atapour et al., Microstructure and corrosion behavior of multipass gas tungsten arc welded 304L stainless steel. Mater. Des. **55**, 905–911 (2014). https://doi.org/10.1016/j.matdes.2013.10.064
14. R. Unnikrishnan, K.S.N. Satish Idury, T.P. Ismail et al., Effect of heat input on the microstructure, residual stresses and corrosion resistance of 304L austenitic stainless steel weldments. Mater. Charact. **93**, 10–23 (2014). https://doi.org/10.1016/j.matchar.2014.03.013
15. X.L. Wei, X. Ling, Investigation of welded structures on mechanical properties of 304L welded tube-to-tubesheet joints. Eng. Fail. Anal. **52**, 90–96 (2015). https://doi.org/10.1016/j.engfailanal.2015.03.003
16. R.K. Desu, H.N. Krishnamurthy, A. Balu et al., Mechanical properties of Austenitic Stainless Steel 304L and 316L at elevated temperatures. J. Mater. Restechnol. **5**, 13–20 (2016). https://doi.org/10.1016/j.jmrt.2015.04.001
17. Z. Wang, T.A. Palmer, A.M. Beese, Effect of processing parameters on microstructure and tensile properties of austenitic stainless steel 304L made by directed energy deposition additive manufacturing. Acta Mater. **110**, 226–235 (2016). https://doi.org/10.1016/j.actamat.2016.03.019
18. G.G. Scatigno, M.P. Ryan, F. Giuliani et al., The effect of prior cold work on the chloride stress corrosion cracking of 304L austenitic stainless steel under atmospheric conditions. Mater. Sci. Eng. A **668**, 20–29 (2016). https://doi.org/10.1016/j.msea.2016.05.037
19. D. Özyürek, An effect of weld current and weld atmosphere on the resistance spot weldability of 304L austenitic stainless steel. Mater. Des. **29**, 597–603 (2008). https://doi.org/10.1016/j.matdes.2007.03.008
20. I. Akkurt, Effective atomic and electron numbers of some steels at different energies. Ann. Nucl. Energy **36**, 1702–1705 (2009). https://doi.org/10.1016/j.anucene.2009.09.005
21. V.P. Singh, N.M. Badiger, Study of mass attenuation coefficients, effective atomic numbers and electron densities of carbon steel and stainless steels. Radioprotection **48**, 431–443 (2013). https://doi.org/10.1051/radiopro/2013067
22. V.P. Singh, M.E. Medhat, S.P. Shirmardi, Comparative studies on shielding properties of some steel alloys using Geant4, MCNP, WinXCOM and experimental results. Radiat. Phys. Chem. **106**, 255–260 (2015). https://doi.org/10.1016/j.radphyschem.2014.07.002
23. M.E. Medhat, Y. Wang, Investigation on radiation shielding parameters of oxide Dispersion strengthened steels used in high temperature nuclear reactor applications. Ann. Nucl. Energy **80**, 365–370 (2015). https://doi.org/10.1016/j.anucene.2015.01.044
24. M.M. Eissa, S.U. El-kameesy, S.A. El-Fiki et al., Attenuation capability of low activation-modified high manganeseaustenitic stainless steel for fusion reactor system. Fus. Eng. Des. **112**, 130–135 (2016). https://doi.org/10.1016/j.fusengdes.2016.08.002
25. D.F. Jackson, D.J. Hawkes, X-ray attenuation coefficients of elements and mixtures. Phys. Rep. **70**, 169–233 (1981). https://doi.org/10.1016/0370-1573(81)90014-4
26. L. Gerward, N. Guilbert, K.B. Jensen et al., WinXCom—a program for calculating X-ray attenuation coefficients. Radiat. Phys. Chem. **71**, 653–654 (2004). https://doi.org/10.1016/j.radphyschem.2004.04.040
27. I. Akkurt, H. Akyıldırım, B. Mavi et al., Photon attenuation coefficients of concrete includes barite in different rate. Ann. Nucl. Energy **37**, 910–914 (2010). https://doi.org/10.1016/j.anucene.2010.04.001
28. S. Kaewjang, U. Maghanemi, S. Kothan et al., New gadolinium based glasses for gamma-rays shielding materials. Nucl. Energy Des. **280**, 21–26 (2014). https://doi.org/10.1016/j.nucengdes.2014.08.030
29. I.I. Bashter, Calculation of radiation attenuation coefficients for shielding concretes. Ann. Nucl. Energy **24**, 1389–1401 (1997). https://doi.org/10.1016/S0306-4549(97)00003-0
30. K. Kaur, K.J. Singh, V. Anand, Correlation of gamma ray shielding and structural properties of PbO–BaO–P_2O_5 glass system. Nucl. Eng. Des. **285**, 31–38 (2015). https://doi.org/10.1016/j.nucengdes.2014.12.033